Coupled-channels analyses for large-angle quasi-elastic scattering in massive systems

Muhammad Zamrun F. and K. Hagino
Department of Physics, Tohoku University, Sendai 980-8578, Japan

S. Mitsuoka and H. Ikezoe
Advanced Science Research Center, Japan Atomic Energy Agency, Tokai, Ibaraki 319-1195, Japan

(Received 3 December 2007; published 12 March 2008)

We discuss in detail the coupled-channels approach for large-angle quasi-elastic scattering in massive systems, where many degrees of freedom may be involved in the reaction. We especially investigate the effects of single-, double-, and triple-phonon excitations on the quasi-elastic scattering for ^{48}Ti, ^{54}Cr, ^{56}Fe, ^{64}Ni, and ^{70}Zn+^{208}Pb systems, for which the experimental cross sections have been measured recently. We show that the present coupled-channels calculations well account for the overall width of the experimental barrier distribution for these systems. In particular, it is shown that the calculations taking into account single-quadrupole phonon excitation in ^{48}Ti and triple-octupole phonon excitations in ^{208}Pb reasonably well reproduce the experimental quasi-elastic cross section and barrier distribution for the ^{48}Ti+^{208}Pb reaction. However, ^{54}Cr, ^{56}Fe, ^{64}Ni, and ^{70}Zn+^{208}Pb systems seem to require the double-quadrupole phonon excitations in the projectiles to reproduce the experimental data.

DOI: 10.1103/PhysRevC.77.034604 PACS number(s): 24.10.Eq, 25.60.Pj, 25.70.Bc, 27.80.+w

I. INTRODUCTION

It is now well established that the internal structure of colliding nuclei strongly influences heavy-ion collisions at energies around the Coulomb barrier [1–4]. In particular, the coupling to the collective excitations (rotation and vibrational states) in the target and projectile nuclei participating in the reaction significantly enhances the fusion cross sections for intermediate mass systems. Such couplings give rise to a distribution of the Coulomb barrier [1,2,5], which can most easily be visualized for reactions involving a deformed nucleus. In this case, the nucleus-nucleus potential depends on the orientation angle of the deformed nucleus with respect to the beam direction. Because the orientation angle distributes isotropically at the initial stage of the reaction, so does the potential barrier. The concept of barrier distribution can be extended also to systems with a nondeformed target [5], where the distribution originates from the coupling between the relative motion and vibrational excitations in the colliding nuclei and/or transfer processes. Notice that although this concept is exact only when the excitation energy is zero, to a good approximation it holds also for systems with a nonzero excitation energy [6,7].

In Ref. [8], Rowley *et al*. argued that the barrier distribution can be directly extracted from a measured fusion cross section, $\sigma_{\rm fus}(E)$, by taking the second derivative of the product $E\sigma_{\rm fus}(E)$ with respect to the center-of-mass energy, E, that is, $D^{\rm fus} = d^2(E\sigma_{\rm fus})/dE^2$. This method has stimulated many high-precision measurements of the fusion excitation function for medium-heavy mass systems [2,9]. The extracted barrier distributions have revealed that the concept indeed holds and the barrier distribution itself provides a powerful tool for investigating the effects of channel coupling on heavy-ion fusion reactions at sub-barrier energies. It has also been shown recently that the concept of barrier distribution is still valid even for relatively heavy systems, such as ^{100}Mo+^{100}Mo [10].

A similar barrier distribution can also be extracted from quasi-elastic scattering (a sum of elastic, inelastic, and transfer processes) at backward angles [11,12], that is a good counterpart of the fusion reaction [13]. In this case, the barrier distribution is defined as the first derivative of the ratio of quasi-elastic to the Rutherford cross sections, $d\sigma_{\rm qel}/d\sigma_R$, with respect to E, i.e., $D^{\rm qel} = -d(d\sigma_{\rm qel}/d\sigma_R)/dE$. Because the fusion and the quasi-elastic scattering is related to each other because of the flux conservation, similar information can be obtained from those processes and the similarity between the two representations for the barrier distribution has been shown to hold for several intermediate mass systems [11,12,14].

Recently, the quasi-elastic barrier distribution has been exploited to investigate the entrance channel dynamics for fusion reactions to synthesize superheavy elements [15–18]. It has been shown that the concept of barrier distribution remains valid even for such very heavy systems once the deep-inelastic cross sections are properly taken into account. As is expected, the strong channel coupling effects on the barrier distribution have been observed.

In this article, we carry out a detailed coupled-channels analysis for large-angle quasi-elastic scattering data for ^{48}Ti, ^{54}Cr, ^{56}Fe, ^{64}Ni, and ^{70}Zn+^{208}Pb systems leading to superheavy elements $Z = 104$, 106, 108, 110, and 112, respectively [17,18]. We especially study the role of multiphonon excitations of the target and projectile nuclei, which has been shown to play an important role in quasi-elastic scattering for the ^{86}Kr+^{208}Pb system [16].

The article is organized as follows. We briefly explain the coupled-channels formalism for quasi-elastic scattering in Sec. II. We present the results of our systematic analysis in Sec. III. We then summarize the article in Sec. IV.

II. COUPLED-CHANNELS FORMALISM FOR LARGE-ANGLE QUASI-ELASTIC SCATTERING

In this section, we briefly describe the coupled-channels formalism for large-angle quasi-elastic scattering that includes the effects of the vibrational excitations of the colliding nuclei. The total Hamiltonian of the system is assumed to be

$$H = -\frac{\hbar^2}{2\mu}\nabla^2 + V_N^{(0)}(r) + \frac{Z_P Z_T e^2}{r} + H_{\rm exct} + V_{\rm coup}(\boldsymbol{r}, \xi_P, \xi_T), \quad (1)$$

where $\boldsymbol{r}$ is the coordinate of the relative motion between the target and the projectile nuclei, μ is the reduced mass, and ξ_T and ξ_P represent the coordinate of the vibration in the target and the projectile nuclei, respectively. Z_P and Z_T are the atomic number of the projectile and the target, respectively, and $V_N^{(0)}$ is the bare nuclear potential, which we assume to have a Woods-Saxon shape. It consists of the real and imaginary parts, $V_N^{(0)}(r) = V_0(r) + iW_0(r)$. $H_{\rm exct}$ describes the excitation spectra of the target and projectile nuclei, whereas $V_{\rm coup}(\boldsymbol{r}, \xi_P, \xi_T)$ is the potential for the coupling between the relative motion and the vibrational motions of the target and projectile nuclei.

In the isocentrifugal approximation [1,19,20], where the angular momentum of the relative motion in each channel is replaced with the total angular momentum J (in the literature, this approximation is also referred to as the rotating frame approximation or the no-Coriolis approximation), the coupled-channels equations derived from the Hamiltonian (1) read

$$\left[-\frac{\hbar^2}{2\mu}\frac{d^2}{dr^2} + \frac{J(J+1)\hbar^2}{2\mu r^2} + V_N^{(0)}(r) + \frac{Z_P Z_T e^2}{r} - E + \epsilon_n\right] \times u_n(r) + \sum_{n'} V_{nn'}(r) u_{n'}(r) = 0, \quad (2)$$

where ϵ_n is the eigenvalue of the operator $H_{\rm exct}$ for the n-th channel. $V_{nn'}(r)$ is the matrix elements for the coupling potential $V_{\rm coup}$.

In the calculations presented below, we use the method of the computer code CCFULL [19] and replace the vibrational coordinates ξ_P and ξ_T in the coupling potential $V_{\rm coup}$ with the dynamical excitation operators $\hat{O}_P$ and $\hat{O}_T$. The coupling potential is then represented as

$$V_{\rm coup}(r, \hat{O}_P, \hat{O}_T) = V_C(r, \hat{O}_P, \hat{O}_T) + V_N(r, \hat{O}_P, \hat{O}_T), \quad (3)$$

$$V_C(r, \hat{O}_P, \hat{O}_T) = \left[\frac{3R_P^{\lambda_P}\hat{O}_P}{(2\lambda_P+1)r^{\lambda_P}} + \frac{3R_T^{\lambda_T}\hat{O}_T}{(2\lambda_T+1)r^{\lambda_T}}\right] \times \frac{Z_P Z_T e^2}{r}, \quad (4)$$

$$V_N(r, \hat{O}_P, \hat{O}_T) = \frac{-V_0}{\left\{1+\exp\left[\frac{r-R_0-(R_P\hat{O}_P+R_T\hat{O}_T)}{a}\right]\right\}} - V_N^{(0)}(r). \quad (5)$$

Here, λ_P and λ_T denote the multipolarity of the vibrations in the projectile and the target nuclei, respectively. We have subtracted $V_N^{(0)}(r)$ in Eq. (5) to avoid the double counting.

If we truncate the phonon space up to the triple-phonon states (that is, $n = 0$, 1, 2, and 3), the matrix elements of the excitation operator $\hat{O}$ in Eqs. (4) and (5) are given by

$$O_{nn'} = \frac{1}{\sqrt{4\pi}}\begin{bmatrix} 0 & \beta & 0 & 0 \\ \beta & 0 & \sqrt{2}\beta & 0 \\ 0 & \sqrt{2}\beta & 0 & \sqrt{3}\beta \\ 0 & 0 & \sqrt{3}\beta & 0 \end{bmatrix}, \quad (6)$$

where β is the deformation parameter that can be estimated from a measured electric transition probability from the single-phonon state ($n = 1$) to the ground state ($n = 0$). We have assumed the harmonic oscillator model for the vibrations, where ϵ_n in Eq. (2) is given by $\epsilon_n = n\hbar\omega$.

The coupled-channels equations, Eq. (2), are solved with the scattering boundary condition for $u_n(r)$,

$$u_n(r) \to \frac{i}{2}\left[H_J^{(-)}(k_n r)\delta_{n,n_i} - \sqrt{\frac{k_i}{k_n}} S_n^J H_J^{(+)}(k_n r)\right], \quad (r \to \infty) \quad (7)$$

where S_n^J is the nuclear S matrix. $H_J^{(-)}(kr)$ and $H_J^{(+)}(kr)$ are the incoming and the outgoing Coulomb wave functions, respectively. The channel wave number k_n is given by $\sqrt{2\mu(E-\epsilon_n)/\hbar^2}$, and $k_i = k_{n_i} = \sqrt{2\mu E/\hbar^2}$. The scattering angular distribution for the channel n is then given by [20]

$$\frac{d\sigma_n}{d\Omega} = \frac{k_n}{k_i}|f_n(\theta)|^2 \quad (8)$$

with

$$f_n(\theta) = \sum_J e^{[\sigma_J(E)+\sigma_J(E-\epsilon_n)]}\sqrt{\frac{2J+1}{4\pi}}Y_{J0}(\theta) \times \frac{-2i\pi}{\sqrt{k_i k_n}}\left(S_n^J - \delta_{n,n_i}\right) + f_C(\theta)\delta_{n,n_i}, \quad (9)$$

where $\sigma_J(E)$ and $f_C(\theta)$ are the the Coulomb phase shift and the Coulomb scattering amplitude, respectively. The differential quasi-elastic cross section is then calculated to be

$$\frac{d\sigma^{\rm qel}}{d\Omega} = \sum_n \frac{d\sigma_n}{d\Omega}. \quad (10)$$

We will apply this formalism in the next section to analyze the quasi-elastic scattering data of ^{48}Ti, ^{54}Cr, ^{56}Fe, ^{64}Ni, and ^{70}Zn+^{208}Pb systems.

III. COMPARISON WITH EXPERIMENTAL DATA: EFFECTS OF MULTIPHONON EXCITATIONS

In this section, we present the results of our detailed coupled-channels analysis for quasi-elastic-scattering data of ^{48}Ti, ^{54}Cr, ^{56}Fe, ^{64}Ni, and ^{70}Zn+^{208}Pb systems [17,18]. The calculations are performed with a version [21] of the coupled-channels code CCFULL [19]. Notice that the isocentrifugal approximation employed in this code works well for quasi-elastic scattering at backward angles [12]. In the code, the regular boundary condition is imposed at the origin instead of the incoming wave boundary condition. We discuss the

TABLE I. The depth parameter for the real part of the nuclear potential for the ^{48}Ti, ^{54}Cr, ^{56}Fe, ^{64}Ni, and ^{70}Zn+^{208}Pb systems. The radius and the diffuseness parameters are taken to be $r_0 = 1.22$ fm and $a = 0.63$ fm, respectively, for all the systems. The resultant barrier height energy V_B is also listed.

System	V_0(MeV)	V_B(MeV)
^{48}Ti+^{208}Pb	88.90	190.50
^{54}Cr+^{208}Pb	91.70	205.50
^{56}Fe+^{208}Pb	92.85	222.50
^{64}Ni+^{208}Pb	95.10	236.25
^{70}Zn+^{208}Pb	108.2	249.30

stability of the numerical calculations for the massive systems in Appendix.

The surface diffuseness of the real part of the nuclear potential is taken to be $a = 0.63$ fm, as suggested by recent studies on deep sub-barrier quasi-elastic and Mott scattering [22–24], whereas the radius parameter to be $r_0 = 1.22$ fm for all the systems. Notice that a similar value for a has been used also in the analysis of the recent experimental data for the quasi-elastic scattering in the ^{86}Kr+^{208}Pb system [16]. The depth parameter, V_0, is adjusted to reproduce the experimental quasi-elastic cross sections for each system. The optimum values of the depth parameter and the resultant Coulomb barrier height are summarized in Table I. As usually done, we use a short range imaginary potential with $W_0 = 30$ MeV, $r_w = 1.0$ fm, and $a_w = 0.3$ fm to simulate the compound nucleus formation. The results are insensitive to these parameters as long as the imaginary part of the potential is well confined inside the Coulomb barrier. The excitation energy and the corresponding deformation parameter for the single-phonon excitation in each nucleus included in the calculations are given in Table II. The latter quantity is taken from Refs. [25,26]. The radius of the target and the projectile are taken to be $R_T = 1.2A_T^{1/3}$ and $R_P = 1.2A_P^{1/3}$, respectively, to be consistent with the deformation parameters [25,26]. All the calculations shown below are performed at the scattering angle of $\theta_{\rm c.m.} = 170^\circ$. We plot the quasi-elastic cross sections

TABLE II. The properties of the single-phonon states included in the present coupled-channels calculations. $\hbar\omega$ and β are the excitation energy and the dynamical deformation parameter, respectively.

Nucleus	I^π	$\hbar\omega$ (MeV)	β
^{208}Pb	3^-	2.614	0.110[a]
^{48}Ti	2^+	0.983	0.269[b]
^{54}Cr	2^+	0.834	0.250[b]
^{56}Fe	2^+	0.846	0.239[b]
^{64}Ni	2^+	1.346	0.179[b]
^{70}Zn	2^+	0.884	0.228[b]

[a]From Ref. [25].
[b]From Ref. [26].

and barrier distributions as a function of the effective energy defined by [11,12]

$$E_{\rm eff} = 2E\frac{\sin(\theta/2)}{1+\sin(\theta/2)}, \tag{11}$$

which takes into account the centrifugal energy. We calculate the quasi-elastic barrier distributions from the cross sections in a similar way as the one used to obtain the experimental barrier distributions [18]. Namely, we use the point difference formula with the energy step of $\Delta E = 0.25$ MeV and then smooth the resultant barrier distribution with the Gaussian function with the full width at half maximum (FWHM) of 1.5 MeV. We have checked that the shape of the barrier distribution does not change significantly even if we use a larger energy step for the point difference formula, e.g., $\Delta E = 0.5$ MeV.

A. Effect of double-phonon excitations

Let us first discuss the effect of double-octupole phonon excitations in the ^{208}Pb target. Such excitations have been shown to play a significant role in the sub-barrier fusion reaction between ^{16}O and ^{208}Pb nuclei [27,28].

The dotted line in Fig. 1 shows the result of the coupled-channels calculations for the ^{48}Ti+^{208}Pb system obtained by taking into account the coupling to the single-octupole phonon state in the target nucleus, ^{208}Pb, and the single-quadrupole phonon state in the projectile nucleus, ^{48}Ti. The mutual excitations in the projectile and the target nuclei are fully taken into account in this calculation as well as in all the other calculations presented in this article. Figures 1(a) and 1(b) show the ratio of the quasi-elastic to the Rutherford cross sections, $d\sigma_{\rm qel}/d\sigma_R$, and the quasi-elastic barrier distribution, $D^{\rm qel}$, respectively. Although the overall width of the barrier distribution is reproduced reasonably well with this calculation, the detailed structure is somewhat inconsistent with the experimental data. The situation is similar even when we include the double-quadrupole phonon states in the projectile while keeping the single-octupole phonon coupling in the target nucleus (not shown). We then investigate the effect of the double-octupole phonon couplings in the target nucleus. The solid and the dashed lines in Fig. 1 show the results with the single- and the double-quadrupole phonon excitations in the projectile, respectively, where as the double-octupole phonon couplings in the target is included in both the calculations. The former calculation reproduces both the cross sections and the barrier distribution reasonably well, although the latter calculation somehow worsens the agreement. This clearly suggests that the double-octupole phonon excitations in the target nucleus is important in the quasi-elastic ^{48}Ti+^{208}Pb scattering. We summarize the χ^2 value of our calculations in Table III.

Because the coupling to the one-quadrupole phonon state in the projectile and the two-octupole phonon states in the target reasonably well reproduce the experimental quasi-elastic scattering data for the ^{48}Ti+^{208}Pb system, one may expect that the same coupling scheme accounts for the experimental data for the other systems, ^{54}Cr, ^{56}Fe, ^{64}Ni, and ^{70}Zn+^{208}Pb. The results of the coupled-channels calculations with this coupling

TABLE III. The value of χ^2 for the quasi-elastic cross sections for the ^{48}Ti+^{208}Pb system obtained with the coupled-channels calculations with various coupling schemes. The coupling schemes are denoted as $[n_2, n_3]$, where n_2 is the number of quadrupole phonon excitation in the projectile nucleus, whereas n_3 is the number of octupole phonon in the target nucleus.

System	[1,1]	[1,2]	[1,3]	[2,2]
^{48}Ti+^{208}Pb	19.15	9.82	7.12	37.12

scheme is shown by the dashed line in Fig. 2. Figures 2(a), 2(c), 2(e), and 2(g) are for the quasi-elastic cross sections for the ^{54}Cr, ^{56}Fe, ^{64}Ni, and ^{70}Zn+^{208}Pb systems, respectively, whereas Figs. 2(b), 2(d), 2(f), and 2(h) are for the quasi-elastic barrier distributions. One can clearly see that these calculations underestimate the experimental cross sections at high energies, although the experimental barrier distributions themselves are reproduced reasonably well. We repeat the same calculations by including the coupling up to the double-quadrupole phonon

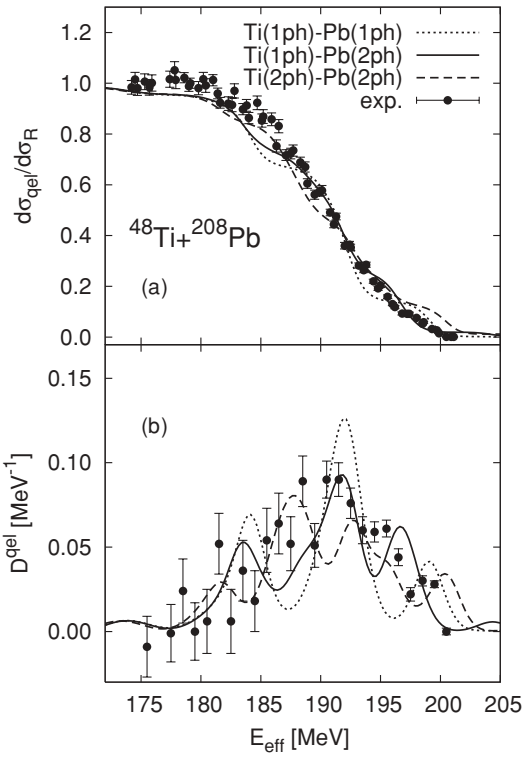

FIG. 1. Effects of multiphonon excitations on the quasi-elastic scattering cross section (upper panel) and on the quasi-elastic barrier distribution (lower panel) for the ^{48}Ti+^{208}Pb system. The dotted line is the result of the coupled-channels calculations, including coupling to the one-quadrupole phonon state in the projectile and the one-octupole phonon states in the target nucleus, whereas the solid line is obtained by including the coupling in addition to the two-octupole phonon state in the target nucleus. The dashed line is the result of double-quadrupole phonon couplings in the projectile and the double-octupole phonon couplings in the target nucleus. The experimental data are taken from Ref. [18].

TABLE IV. Same as in Table III but for the ^{54}Cr, ^{56}Fe, ^{64}Ni and ^{70}Zn+^{208}Pb systems.

System	[1,2]	[1,3]	[2,2]	[2,3]
^{54}Cr+^{208}Pb	52.47	49.80	20.61	11.78
^{56}Fe+^{208}Pb	28.46	28.36	10.44	10.28
^{64}Ni+^{208}Pb	57.45	61.43	32.21	30.64
^{70}Zn+^{208}Pb	26.52	24.81	11.36	6.87

states in the projectile, in addition to the double-octupole phonon states in the target nucleus. These results are shown by the solid in Fig. 2. The agreement with the experimental data is considerably improved, especially for the quasi-elastic cross sections. See Table IV for the χ^2 values. It is thus evident that the coupling to the double-quadrupole phonon states in the projectile is needed to explain the experimental data for the ^{54}Cr, ^{56}Fe, ^{64}Ni, and ^{70}Zn+^{208}Pb reactions.

The reason why the double-quadrupole phonon coupling is not necessary for the ^{48}Ti projectile, whereas it is for the heavier projectiles, is not clear at this moment. This might reflect some ambiguity of the Monte Carlo reaction simulation code LINDA [29], which was used to subtract the deep-inelastic component from the experimental yields at backward angles [18]. Clearly, a further investigation is still necessary concerning the effect of deep inelastic scattering on quasi-elastic scattering in massive systems [15–18].

B. Effect of triple-phonon excitations

In the previous subsection, we showed that the double-octupole phonon excitations in the ^{208}Pb target play an important role in the quasi-elastic scattering for the systems considered in this article. However, the calculated quasi-elastic barrier distributions have a much more prominent peak than the experimental distribution at high energies. Because it has been shown in Refs. [15,16] that the triple-octupole phonon excitations of the ^{208}Pb play a significant role in the large-angle quasi-elastic scattering between ^{86}Kr and ^{208}Pb nuclei, it is intriguing to investigate such effects in the present systems as well.

The results of the coupled-channels calculations, including the coupling to the triple-octupole phonon states in ^{208}Pb for the ^{48}Ti+^{208}Pb reaction, is presented in Fig. 3. The dashed line is the same as the solid line in Fig. 1, that is, the result of the single phonon in ^{48}Ti and double phonons in ^{208}Pb. The solid line denotes the results of the triple-phonon coupling in the target in addition to the single phonon in the projectile. By including the triple-octupole phonons in the target nucleus, the quasi-elastic cross sections are improved slightly (see also Table III). However, one can see that the agreement for the barrier distribution with the experimental data is much improved by the triple-phonon coupling.

The results for the other systems, the ^{54}Cr, ^{56}Fe, ^{64}Ni, and ^{70}Zn+^{208}Pb reactions, are shown in Fig. 4. Figures 4(a), 4(c), 4(e), and 4(g) show the quasi-elastic cross sections, whereas

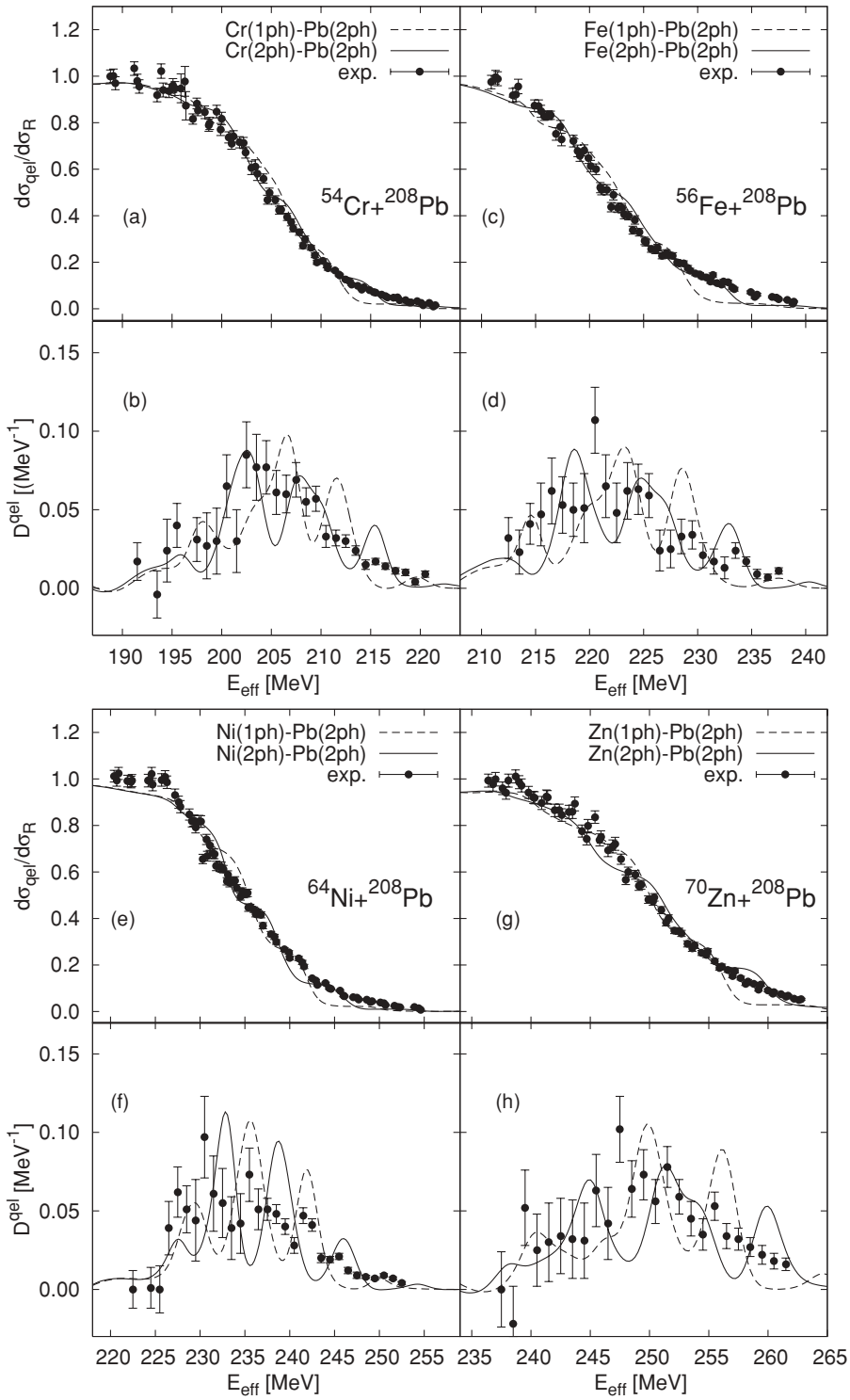

FIG. 2. The quasi-elastic scattering cross sections [(a), (c), (e), and (g)] and the quasi-elastic barrier distributions [(b), (d), (f), and (h)] for the ^{54}Cr, ^{56}Fe, ^{64}Ni, and ^{70}Zn+^{208}Pb systems obtained with two coupling schemes as indicated in the insets. The dashed line is obtained by including the one-quadrupole phonon state in the projectile nuclei, whereas the solid line is obtained with the double-phonon couplings. The double-octupole phonon excitations in the target nucleus is included in all the calculations. The experimental data are taken from Ref. [18].

Figs. 4(b), 4(d), 4(f) and 4(h) show the quasi-elastic barrier distributions. Let us first discuss the calculations with the single-phonon excitation in the projectile. The dotted line in the figures is obtained by taking the coupling to the single-phonon state in the projectile and the triple-octupole phonon excitations in the target. This calculation underestimates the quasi-elastic cross sections at high energies and the obtained barrier distribution is inconsistent with the experimental data. Therefore, the previous results shown in Fig. 2 are not improved even if the triple-phonon excitations in the target are taken into account as long as only the single-phonon excitation is considered for the projectile nucleus. The results with the double-phonon couplings in the projectile together with the triple-phonon excitations in the target are then shown by the

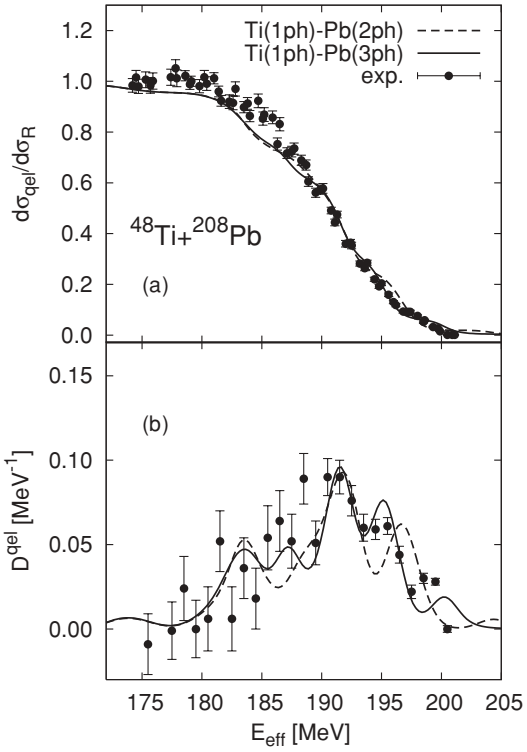

FIG. 3. Effects of triple-phonon excitations on the quasi-elastic scattering cross section (upper panel) and on the quasi-elastic barrier distribution (lower panel) for the ^{48}Ti+^{208}Pb system. The dashed line is the result of the coupled-channels calculations taking into account the coupling to the one-phonon state in the projectile and the two-phonon states in the target nuclei. The solid line is obtained by including the coupling to the one-phonon state in the projectile and the three-phonon states in the target. The experimental data are taken from Ref. [18].

solid line in the figure. For comparison, we also show with the dashed line the results of the double-phonon excitations in both the projectile and the target nuclei, which is the same as the solid line in Fig. 2. One can observe that the inclusion of the triple-octupole phonon excitations in the ^{208}Pb somewhat improves the agreement between the calculations and the experimental data for both the quasi-elastic cross sections and the barrier distributions (see also Table IV).

In Ref. [16], Ntshangase *et al*. reduced the coupling strength of $(3^-) \rightarrow (3^-)^2$ states in ^{208}Pb by a factor of (0.6) and that of $(3^-)^2 \rightarrow (3^-)^3$ by $(0.6)^2$ to explain the experimental barrier distribution for the ^{86}Kr + ^{208}Pb reaction. To see whether such reduction of the coupling strengths improves the agreement between the coupled-channels calculations and the experimental data for the present systems, we repeat the calculations by including those effects for the ^{70}Zn+^{208}Pb system. The results are shown in Fig. 5. The solid line is obtained by reducing the coupling strengths as Ntshangase *et al*. did, whereas the dashed line is the same as the solid line in Figs. 4(g) and 4(h), that is, obtained by assuming the harmonic limit. In both cases, we take into account the coupling to the double-quadrupole phonon excitations in the projectile nucleus. One can see that the harmonic model leads to a better agreement with the experimental data both for the cross sections and the barrier distribution, as compared to the anharmonic calculations. The difference between Ref. [16] and the present calculations concerning the role of anharmonicity may originate from the fact that Ref. [16] used a smaller value for R_T ($= 1.06A_T^{1/3}$ fm) and thus a larger value for β_3($= 0.16$). To clarify the role of anharmonicity of multiphonon excitations in quasi-elastic scattering in massive systems, it would be required to take into account also the reorientation terms [14,30,31]. It is beyond the scope of this article, and we will leave it for a future study.

C. Surface diffuseness of the nuclear potential

We next discuss the dependence of the quasi-elastic scattering on the surface diffuseness parameter of the nuclear potential. The standard value for the diffuseness parameter is around 0.63 fm [32–34]. Recently, systematic studies on quasi-elastic scattering as well as Mott scattering at deep sub-barrier energies have revealed that the surface region of the nuclear potential is indeed consistent with the standard value of the surface diffuseness parameter [22–24]. However, it has been known for some time that the recent high-precision data of sub-barrier fusion cross sections require a larger value of surface diffuseness parameter, ranging between 0.75 and 1.5 fm [35]. Because the large-angle quasi-elastic scattering around the Coulomb barrier may probe both the surface region and the inner part of the nuclear potential, it is interesting to study the sensitivity of the quasi-elastic cross sections and barrier distributions to the surface diffuseness parameter.

For this purpose, as an example, we repeat the coupled-channels calculations for the ^{64}Ni + ^{208}Pb reaction using the nuclear potential with $a = 1.0$ fm. We readjust the depth and the radius parameters to be $V_0 = 160.70$ MeV and $r_0 = 1.10$ fm, respectively, so that the barrier height remains the same as the one listed in Table I. We include the coupling up to the double-phonon states in the projectile and the triple-phonon states in the target. Figure 6 compares the results with $a = 0.63$ fm (the solid line) to the one with $a = 1.0$ fm (the dashed line). One sees that the calculations with $a = 1.0$ fm underestimate the quasi-elastic cross section, although the shape of barrier distribution itself is similar to the one obtained with $a = 0.63$ fm. The dotted line is obtained with the same value of surface diffuseness parameter $a = 1.0$ fm as the one for the dashed line, but by changing the depth parameter V_0 so that the resultant barrier height is higher by 2.4 MeV. This calculation now reproduces the experimental quasi-elastic cross sections at energies larger than $E_{\text{c.m.}} = 230$ MeV reasonably well, but below this energy the cross sections are underestimated. Therefore, it seems difficult to reproduce the experimental quasi-elastic cross sections with the diffuseness parameter of $a = 1.0$ fm at energies below and above the Coulomb barrier simultaneously. We have checked that the situation is similar for the other systems, ^{48}Ti, ^{54}Cr, ^{56}Fe, and ^{70}Zn+^{208}Pb. This result clearly indicates that the standard value of surface diffuseness, $a = 0.63$ fm, is preferred by the experimental quasi-elastic scattering data for the systems studied in this article.

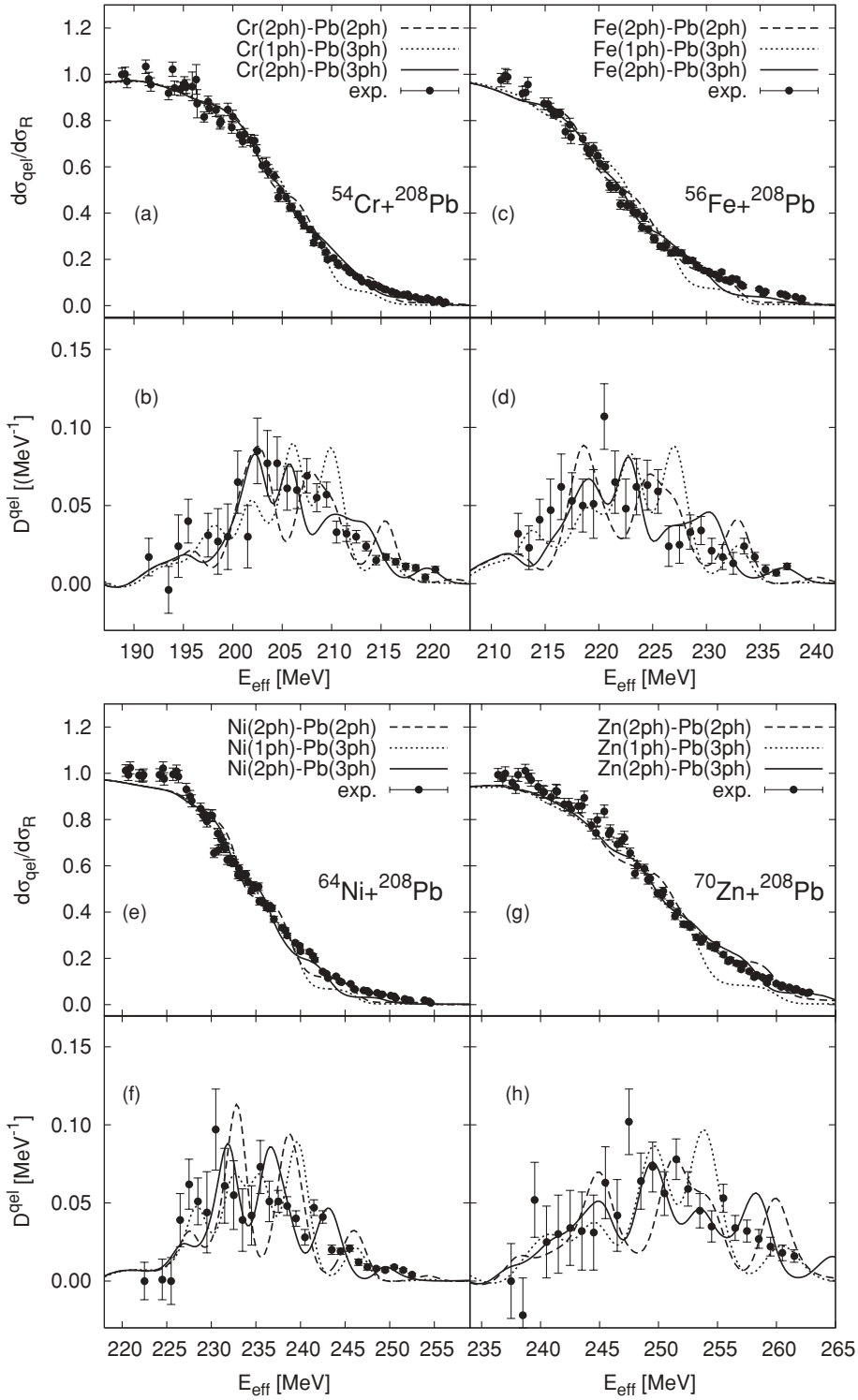

FIG. 4. Effects of triple-phonon excitations on the quasi-elastic cross sections [(a), (c), (e), and (g)] and on the quasi-elastic barrier distributions [(b), (d), (f), and (h)] for the ^{54}Cr, ^{56}Fe, ^{64}Ni, and ^{70}Zn+^{208}Pb systems. The dashed line is the same as the solid line in Fig. 2, whereas the dotted line is the results of the calculations taking the coupling to the triple-octupole phonon in the target and the one-quadrupole phonon state in the projectile nucleus into account. The solid line is obtained by including the coupling to the double-quadrupole phonon states in the projectile and the triple-otcupole phonon states in the target nucleus. The experimental data are taken from Ref. [18].

D. Comparison between quasi-elastic and fusion barrier distributions

An interesting question is how well the quasi-elastic barrier distributions studied in this article can be compared with the corresponding fusion barrier distributions. Such study has been carried out for medium-heavy systems [11,12,14], which showed that the fusion and quasi-elastic barrier distributions behave similar to each other within the same coupling scheme considered, although the latter is somewhat more smeared. In this subsection, we discuss to which extent this finding remains the same in the massive systems, where the coupling is stronger and more degrees of freedom are involved.

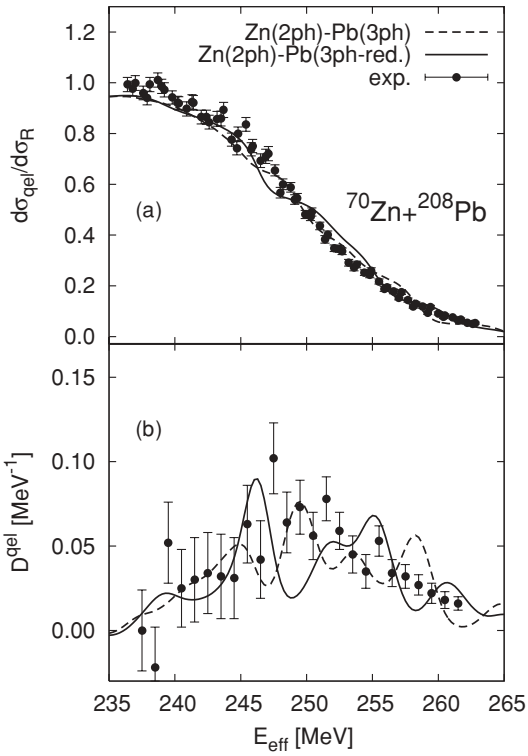

FIG. 5. Effect of anharmonic octupole phonon excitations in ^{208}Pb on (a) the quasi-elastic cross section and (b) the quasi-elastic barrier distribution for the ^{70}Zn+^{208}Pb reaction. The solid line is the coupled-channels calculations obtained by reducing the coupling strengths to multiphonon states, whereas the dashed line denotes the results in the harmonic limit. The experimental data are taken from Ref. [18].

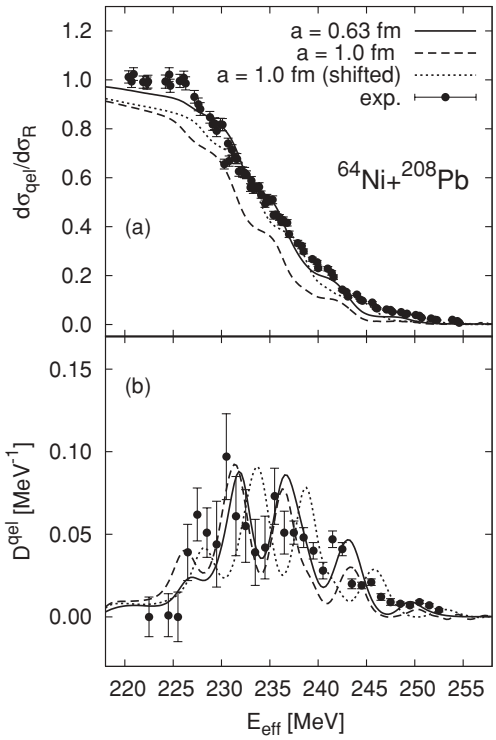

FIG. 6. Comparison of the experimental data with the coupled-channels calculations obtained using different values of the surface diffuseness of the nuclear potential for ^{64}Ni + ^{208}Pb reaction for (a) the quasi-elastic cross section and (b) the quasi-elastic barrier distribution. The solid and the dashed lines are obtained using the surface diffuseness of the nuclear potential $a = 0.63$ fm and $a = 1.0$ fm, respectively. The dotted line is the results obtained by shifting the barrier height by around +2.40 MeV for the calculations using $a = 1.0$ fm. Experimental data is taken from Ref. [18].

Figure 7 compares the quasi-elastic (the solid line) with the fusion (the dashed line) barrier distributions for the ^{48}Ti+^{208}Pb system. The coupling scheme included in the calculations is the same as in Fig. 3, i.e., the single-quadrupole phonon in the projectile as well as the triple-octupole phonon in the target. The comparision for the other systems, ^{54}Cr, ^{56}Fe, ^{64}Ni, and ^{70}Zn+^{208}Pb, are shown in Fig. 8, where the double-quadrupole phonon excitations in the projectile together with the triple-octupole phonon excitations in the target are considered. To compare the two barrier distributions, we plot the quasi-elastic barrier distribution as a function of effective energy defined by Eq. (11). This scaling maps the quasi-elastic barrier distribution obtained at a finite value of angular momentum onto that for the s-wave scattering (i.e., for $\theta = \pi$). Notice that a fusion barrier distribution represents a distribution of barrier heights for the s wave [2]. Moreover, we smear the fusion barrier distribution in the same way as for the quasi-elastic barrier distribution and normalize them to unit area.

From these figures, it is evident that even for the massive systems the quasi-elastic and fusion barrier distributions are rather similar to each other, although the former has more smooth peaks [12]. The peak positions are slightly shifted between the two distributions because of the low-energy tails in the quasi-elastic barrier distributions [12]. These behaviors are

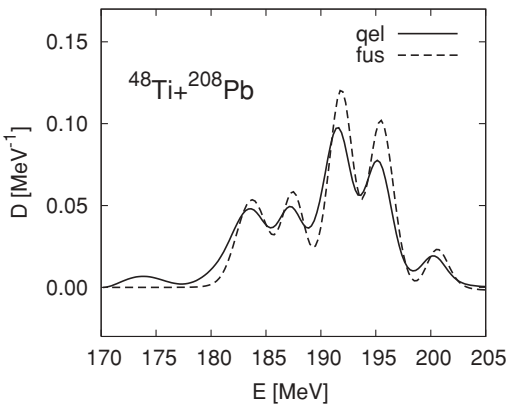

FIG. 7. Comparison of the calculated quasi-elastic (solid line) with fusion (dashed line) barrier distributions for the ^{48}Ti+^{208}Pb reaction. The quasi-elastic barrier distribution is plotted as a function of effective energy $E_{\rm eff}$ defined by Eq. (11) with $\theta = 170^\circ$, whereas the fusion barrier distribution as a function of the center-of-mass (c.m.) energy E. They are normalized to unit area in the energy interval between $E = 170$ and 210 MeV. The single-quadrupole phonon excitation in the projectile and the triple-octupole phonon excitation in the target are taken into account.

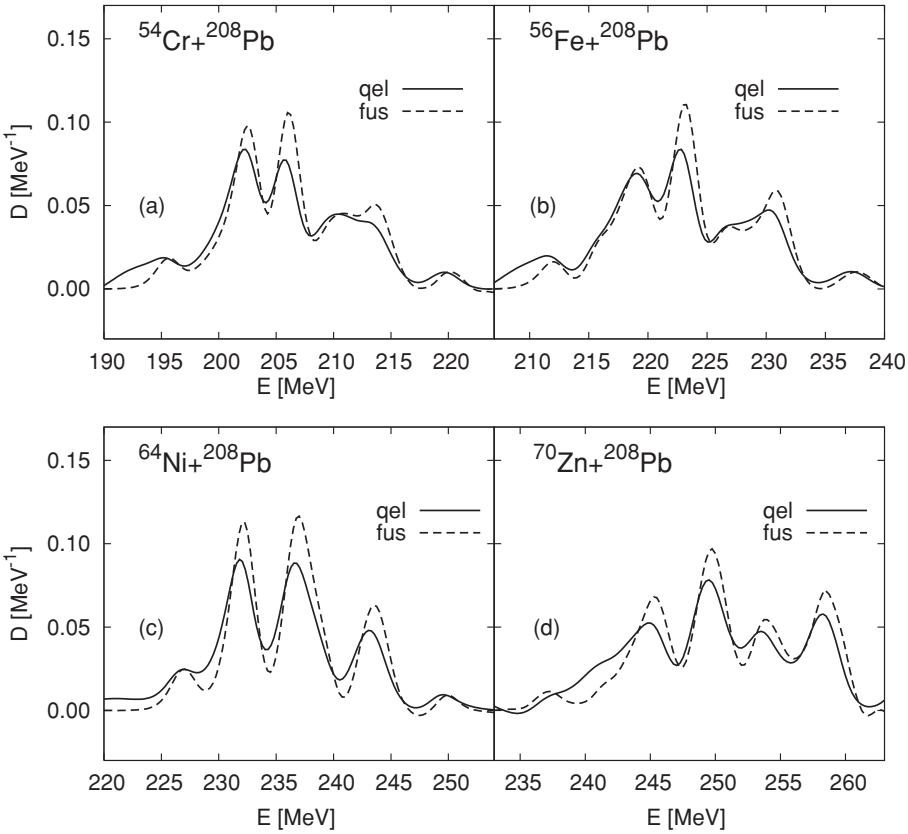

FIG. 8. Same as described in the caption to Fig. 7, but for (a) ^{54}Cr+^{208}Pb, (b) ^{56}Fe+^{208}Pb, (c) ^{64}Ni+^{208}Pb, and (c) ^{70}Zn+^{208}Pb systems. The double-quadrupole phonon excitation in the projectile as well as the triple-octupole phonon excitation in the target are taken into account.

similar to the ones found in the previous studies for medium-heavy mass systems [14].

IV. SUMMARY

We performed a detailed coupled-channels analysis for large-angle quasi-elastic scattering of the ^{48}Ti, ^{54}Cr, ^{56}Fe, ^{64}Ni, and ^{70}Zn+^{208}Pb systems, where their experimental barrier distributions have been extracted recently. Our coupled-channels calculations with multiphonon excitations in the colliding nuclei reproduce the experimental quasi-elastic cross sections as well as the barrier distributions, indicating clearly that the coupled-channels approach still works even for massive systems [10]. It was crucial to subtract properly the deep-inelastic components from the total backward-angle cross sections to reach these agreements between the calculations and the experimental data.

In more details, the calculation with the single-quadrupole phonon excitation in ^{48}Ti and the triple-octupole phonon excitations in ^{208}Pb reproduces reasonably well the experimental data for the ^{48}Ti+^{208}Pb system. However, for the ^{54}Cr, ^{56}Fe, ^{64}Ni, and ^{70}Zn+^{208}Pb systems, we found that the coupling to the double-quadrupole phonon excitations in the projectile nucleus in addition to the coupling to the triple-octupole phonon states in the target nucleus seems to be needed to fit the experimental data. These results suggest that the triple-octupole phonon excitations in the ^{208}Pb nucleus plays an important role in describing the experimental data for the quasi-elastic cross section and the quasi-elastic barrier distribution for the present massive systems. This is consistent with the previous finding for the ^{86}Kr+^{208}Pb system [16].

Although our calculations well reproduce the gross features of the experimental barrier distributions, higher-precision data are still required to study the detailed structure of the barrier distributions, especially the role of multioctupole phonon states in ^{208}Pb. From the theoretical side, a further detailed investigation will also be necessary, taking into account the anharmonicity of the multiphonon excitations.

ACKNOWLEDGMENTS

This work was partly supported by The 21st Century Center of Excellence Program "Exploring New Science by Bridging Particle-Matter Hierarchy" of Tohoku University and partly by Monbukagakusho Grand-in-Aid and Grant-in-Aid for Scientific Research under the program no. 19740115 from the Japanese Ministry of Education, Culture, Sports, Science and Technology.

APPENDIX: NUMERICAL STABILIZATION OF COUPLED-CHANNELS CALCULATION

In this Appendix, we discuss the problem of numerical instability of coupled-channels calculations and the stabilization methods that we employ in the present calculations.

The coupled-channels equations (2) form a set of N second-order coupled linear differential equations, where N is the dimension of the coupled-channels equations. These equations

can be solved by generating N linearly independent solutions and taking a linear combination of these N solutions so that the asymptotic boundary condition, (7), as well as the regular boundary condition at the origin, are satisfied. The linearly independent solutions can be obtained by taking N different sets of initial conditions at $r = 0$. We denote these solutions by $\phi_{nn_i}(r)$, where n refers to the channels, whereas n_i refers to a particular choice of the initial conditions. A simple choice for the N initial conditions is to impose

$$\phi_{nm}(r) \to c r^{J+1} \delta_{n,m}, \quad \text{for} \quad r \to 0, \tag{A1}$$

where c is an arbitrary number and J is the total angular momentum. With these boundary condition, the coupled-channels equations for $\phi_{nm}(r)$ given by

$$\left[-\frac{\hbar^2}{2\mu}\frac{d^2}{dr^2} + \frac{J(J+1)\hbar^2}{2\mu r^2} + V_N^{(0)}(r) + \frac{Z_P Z_T e^2}{r} - E + \epsilon_n \right] \times \phi_{nm}(r) + \sum_{n'} V_{nn'}(r)\phi_{n'm}(r) = 0, \tag{A2}$$

are solved outwards up to a matching radius $R_{\max}$. The wave functions $u_n(r)$ in Eq. (2) are then obtained as

$$u_n(r) = \sum_m C_m \phi_{nm}(r), \tag{A3}$$

where the coefficients C_m are determined so that the asymptotic boundary condition (7) is fulfilled.

In the classical forbidden region, the scattering wave functions exponentially damp as the coordinate r decreases. For the smaller energy, the damping is stronger. Therefore, when the excitation energy ϵ_n is finite, the absolute value of the wave functions for each channel differs by an order of magnitude in the classical forbidden region, and thus the wave functions tend to be dominated by that of the channel that has the smallest excitation energy. This easily destroys the linear independence of the N numerical solutions ϕ_{nm} and causes the numerical instability. This is a serious problem especially when the coupling is strong, as in the massive systems which we discuss in this article.

Several methods have been proposed to stabilize the numerical solution of the coupled-channels equations [36–39]. In the present calculations, we stabilize the solutions by diagonalizing the wave function matrix ϕ_{nm} at several points of r to recover the linear independence. That is, at some radius r_s, we compute the inverse of the matrix $A_{nm} = \phi_{nm}(r_s)$ and define the new set of wave functions,

$$\tilde{\phi}_{nm}(r) = \sum_k \phi_{nk}(r)(A^{-1})_{km}. \tag{A4}$$

The new wave functions $\tilde{\phi}$ obey similar coupled-channels equations as Eq. (A2), with the boundary conditions given by

$$\tilde{\phi}_{nm}(r_s - h) = \sum_k \phi_{nk}(r - h)(A^{-1})_{km}, \tag{A5}$$

$$\tilde{\phi}_{nm}(r_s) = \delta_{n,m}. \tag{A6}$$

Here, h is the step for the discretization of the radial coordinate, r. These coupled-channels equations are solved outwards from r_s. The solutions ϕ can then be constructed as $\phi = A\tilde{\phi}$. We impose this stabilization procedure up to $r = 15$ fm with an interval of 1 fm. Although this method is similar to those in Refs. [38,39], our method is much simpler to implement.

This method is sufficient for intermediate heavy systems, such as ^{16}O+^{144}Sm. For massive systems, however, we still encounter a small numerical instability [40]. To cure this problem, in addition to the stabilization method (A4), we also adopt two other methods, which are used in the computer code FRESCO [41]. That is, we introduce two radii, $R_{\min}$ and R_{cut}. $R_{\min}$ is the radius from which the coupled-channels equations (A2) are solved, i.e., these equations are solved from $r = R_{\min}$ instead of $r = 0$, by setting $\phi_{nm}(r) = 0$ for $r \leqslant R_{\min}$. R_{cut} is a cut-off radius for the coupling matrix, i.e., the off-diagonal components of the coupling matrix $V_{nn'}(r)$ are set to be zero for $r \leqslant R_{\text{cut}}$. Both the procedures are justified when the absorption is strong inside the Coulomb barrier, as in heavy-ion systems, and the results are insensitive to the particular choice of $R_{\min}$ and R_{cut} as long as they are inside the Coulomb barrier. Typically, we take $R_{\min} = 6$ fm and $R_{\text{cut}} = 10$ fm to obtain reasonable results for the present systems (notice that the pocket and the barrier appear at, e.g., 11.3 and 13.2 fm, respectively, for the ^{64}Ni+^{208}Pb system with the nuclear potential given in Table I).

[1] A. B. Balantekin and N. Takigawa, Rev. Mod. Phys. **70**, 77 (1998).
[2] M. Dasgupta, D. J. Hinde, N. Rowley, and A. M. Stefanini, Annu. Rev. Nucl. Part. Sci. **48**, 401 (1998).
[3] L. F. Canto, P. R. S. Gomes, R. Donangelo, and M. S. Hussein, Phys. Rep. **424**, 1 (2006).
[4] N. Keeley, R. Raabe, N. Alamanos, and J. L. Sida, Prog. Part. Nucl. Phys. **59**, 579 (2007).
[5] C. H. Dasso, S. Landowne, and A. Winther, Nucl. Phys. **A405**, 381 (1983); **A407**, 221 (1983).
[6] K. Hagino, N. Takigawa, and A. B. Balantekin, Phys. Rev. C **56**, 2104 (1997).
[7] K. Hagino and A. B. Balantekin, Phys. Rev. A **70**, 032106 (2004).
[8] N. Rowley, G. R. Sacthler, and P. H. Stelson, Phys. Lett. **B254**, 25 (1991).
[9] J. R. Leigh *et al.*, Phys. Rev. C **52**, 3151 (1995).
[10] N. Rowley, N. Grar, and K. Hagino, Phys. Lett. **B632**, 243 (2006).
[11] H. Timmers, J. R. Leigh, M. Dasgupta, D. J. Hinde, R. C. Lemon, J. C. Mein, C. R. Morton, J. O. Newton, and N. Rowley, Nucl. Phys. **A584**, 190 (1995).
[12] K. Hagino and N. Rowley, Phys. Rev. C **69**, 054610 (2004).
[13] M. V. Andres, N. Rowley, and M. A. Nagarajan, Phys. Lett. **B202**, 292 (1988).
[14] Muhammad Zamrun F. and K. Hagino, Phys. Rev. C **77**, 014606 (2008).
[15] N. Rowley *et al.*, Phys. At. Nucl. **79**, 1093 (2006)
[16] S. S. Ntshangase *et al.*, Phys. Lett. **B651**, 27 (2007).
[17] H. Ikezoe *et al.*, AIP Conf. Proc. **853**, 69 (2006).

[18] S. Mitsuoka, H. Ikezoe, K. Nishio, K. Tsuruta, S. C. Jeong, and Y. Watanabe, Phys. Rev. Lett. **99**, 182701 (2007).
[19] K. Hagino, N. Rowley, and A. T. Kruppa, Comput. Phys. Commun. **123**, 143 (1999).
[20] H. Esbensen, S. Landowne, and C. Price, Phys. Rev. C **36**, 1216 (1987); **36**, 2359 (1987).
[21] K. Hagino *et al*. (to be published).
[22] K. Washiyama, K. Hagino, and M. Dasgupta, Phys. Rev. C **73**, 034607 (2006).
[23] L. R. Gasques, M. Evers, D. J. Hinde, M. Dasgupta, P. R. S. Gomes, R. M. Anjos, M. L. Brown, M. D. Rodriguez, R. G. Thomas, and K. Hagino, Phys. Rev. C **76**, 024612 (2007).
[24] D. J. Hinde, R. L. Ahlefeldt, R. G. Thomas, K. Hagino, M. L. Brown, M. Dasgupta, M. Evers, L. R. Gasques, and M. D. Rodriguez, Phys. Rev. C **76**, 014617 (2007).
[25] T. Kibedi and R. H. Spears, At. Data Nucl. Data Tables **80**, 35 (2002).
[26] S. Raman, C. W. Nestor, and P. Tikkanen, At. Data Nucl. Data Tables **78**, 1 (2001).
[27] M. Dasgupta, K. Hagino, C. R. Morton, D. J. Hinde, J. R. Leigh, N. Takigawa, H. Timmers, and J. O. Newton, J. Phys. G **23**, 1491 (1997).
[28] C. R. Morton, A. C. Berriman, M. Dasgupta, D. J. Hinde, J. O. Newton, K. Hagino, and I. J. Thompson, Phys. Rev. C **60**, 044608 (1999).
[29] E. Duek, L. Kowalsky, and John M. Alexander, Comput. Phys. Commun. **34**, 395 (1985).
[30] K. Hagino, N. Takigawa, and S. Kuyucak, Phys. Rev. Lett. **79**, 2943 (1997).
[31] K. Hagino, S. Kuyucak, and N. Takigawa, Phys. Rev. C **57**, 1349 (1998).
[32] R. A. Broglia and A. Winther, *Frontier in Physics Lecture Notes Series: Heavy Ion Reactions* (Addison-Wesley, Redwood City, CA, 1991), Vol. 84.
[33] P. R. Christensen and A. Winther, Phys. Lett. **B65**, 19 (1976).
[34] G. R. Sacthler and W. G. Love, Phys. Rep. **55**, 183 (1979).
[35] J. O. Newton, R. D. Butt, M. Dasgupta, D. J. Hinde, I. I. Gontchar, C. R. Morton, and K. Hagino, Phys. Rev. C **70**, 024605 (2004); Phys. Lett. **B586**, 219 (2004).
[36] W. Brenig, T. Brunner, A. Gross, and R. Russ, Z. Phys. B **93**, 91 (1993); W. Brenig and R. Russ, Surf. Sci. **315**, 195 (1994).
[37] B. R. Johnson, J. Chem. Phys. **69**, 4678 (1978).
[38] Z. H. Levine, Phys. Rev. A **30**, 1120 (1984).
[39] T. N. Rescigno and A. E. Orel, Phys. Rev. A **25**, 2402 (1982).
[40] K. Hagino, AIP Conf. Proc. **891**, 80 (2007).
[41] I. J. Thompson, Comput. Phys. Rep. **7**, 167 (1988).